

# An Event-Triggered Robust Attitude Control of Flexible Spacecraft With Modified Rodrigues Parameters Under Limited Communication

SYED MUHAMMAD AMRR<sup>1</sup>, (Student Member, IEEE), MASHUQ UN NABI<sup>1</sup>, (Member, IEEE),  
AND ATIF IQBAL<sup>2</sup>, (Senior Member, IEEE)

<sup>1</sup>Department of Electrical Engineering, Indian Institute of Technology Delhi, New Delhi 110016, India

<sup>2</sup>Department of Electrical Engineering, Qatar University, Doha, Qatar

Corresponding author: Atif Iqbal (atif.iqbal@qu.edu.qa)

This publication was made possible by Qatar University High Impact grant # [QUHI-CENG-19/20-2] from the Qatar University. The statements made herein are solely the responsibility of the authors. The publication charges are paid by the Qatar National Library, Doha, Qatar.

**ABSTRACT** The attitude regulation of spacecraft using continuous time execution of the control law is not always affordable for the low-cost satellites with limited wireless resources. Of late, within the ambit of control of systems over networks, event-triggered control has proved to be instrumental in ensuring acceptable closed-loop performance while respecting bandwidth constraints of the underlying network. Aligned with these design objectives, a robust event-triggered attitude control algorithm is proposed to regulate the orientation of a flexible spacecraft subjected to parametric uncertainties, external disturbances, and vibrations due to flexible appendages. The control law is developed using a state-dependent single feedback vector, which further assists in obeying the constrained network. The current information of this vector is updated to the onboard controller only when the predefined triggering condition is satisfied. Thus, the control input is updated through communication channel only when there is a need, which ultimately helps in saving the communication resources. The system trajectories, under the proposed approach, are guaranteed to be uniformly ultimately bounded (UUB) in a small neighborhood of origin by using a high gain. Moreover, the practical applicability of the proposed scheme is also proved by showing the Zeno free behavior in the proposed control, i.e., it avoids the accumulation of the triggering sequence. The numerical simulations results are indeed encouraging and illustrate the effectiveness of the designed controller. Moreover, the numerical comparative analysis shows that the proposed approach performs better than periodically sampled data technique and sliding mode-based event-triggered technique.

**INDEX TERMS** Flexible spacecraft, attitude regulation control, limited data transmission, communication constraints, event-trigger, robust control, Zeno behavior, modified Rodrigues parameters (MRP).

## I. INTRODUCTION

The prime objective of an attitude controller is to re-orient the attitude of the spacecraft to the desired orientation. Attitude controllers have been deployed for various space-related operations like surveillance, communication, navigation, docking in a space station and earth observations, etc. These operations require attitude controllers featuring high accuracy, high pointing precision, faster attitude convergence, high stabilization, and maneuvering capabilities, etc. with minimum usage of communication resources [1]–[4].

In furtherance, the spacecraft is also subjected to consistent uncertainties and disturbances. Moreover, modern

spacecrafts are often manufactured by coupling the rigid hub of the spacecraft to the multiple flexible solar arrays as shown in Fig. 1. These are termed as flexible spacecrafts. The attitude maneuvering performance of a flexible spacecraft is greatly affected by the vibrations of flexible appendages due to the coupling between the rigid and flexible structures. So, all the parametric uncertainties, external disturbances, and vibrations pose numerous challenges in the synthesis of an attitude control law ensuring faithful and robust output performance. Therefore, the attitude controllers must be robust and equipped with disturbance rejection properties [2].

The robust attitude control of flexible spacecraft has been a promising research domain and has been studied for the last

The associate editor coordinating the review of this manuscript and approving it for publication was Zhenbao Liu.

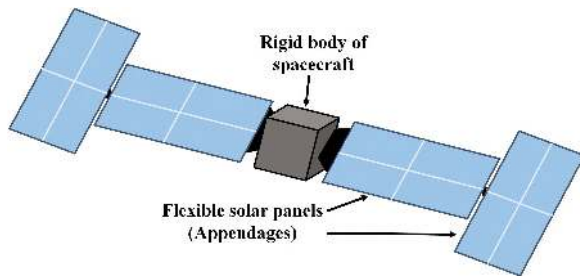


**FIGURE 1.** Sketch of a flexible spacecraft with solar arrays.

two decades. Some of the nonlinear robust control paradigms for the flexible spacecraft are active vibration suppression approach [5], [6], proportional derivative control [7], sliding mode control (SMC) [8]–[10], adaptive control [11]–[13], robust  $H_\infty$  control [14], and disturbance observer based control [15], [16], etc. Although the aforementioned control schemes render satisfactory performance, they are developed in continuous time. Owing to the fact that analytical closed-loop solutions are impossible, the application of these control algorithms to the spacecraft are executed digitally using numerical methods with an extremely small periodic sampling time to mimic the continuous time behavior. Therefore, continuous control schemes are often not physically realizable due to restrictions on hardware support. For instance, a low-cost wireless network has limited data transmission and control of the system over such a network will ultimately lead to the unsatisfactory performance of the closed-loop system. Thus, it is imperative to explore the alternatives to continuous control approach in such scenarios.

In recent years, event-triggered control has emerged as a promising approach aimed at minimizing the number of information transmissions to respect the limited resource constraints of a communication network while stabilizing the system [17]–[19]. The primary difference between the event-triggered approach and the sampled data technique is the aperiodic update of the control signal. In the event-triggered scheme, the control signal is updated at time instants when a predefined state dependent threshold condition is satisfied. These points in time are termed as triggering instants. The control actuation to the spacecraft is fixed between the two consecutive triggering instants.

Lately, results on event-based attitude controller appear in the works [20]–[25] and the references therein. In [20], an event-triggered stabilization of quadrotor without any uncertainties is proposed. Whereas the work in [21] considers attitude regulation of rigid spacecraft affected by external disturbance only. Thereafter, an observer-based event-triggered control is developed to ensure robustness to actuator faults and external disturbances in [22]. An event-triggered scheme is also implemented for the attitude regulation of multiple rigid spacecrafts in [23], [24]. Moreover, in [25], an SMC based event-triggered attitude controller is designed to compensate the effects of external disturbances and

parametric uncertainties while proposing semi-global stability results.

In view of the aforementioned literature, the event-triggered control approaches are only considered for the rigid spacecraft attitude problems which impose fewer design challenges compared to the flexible spacecrafts. Further, the attitude orientation of spacecrafts are also represented by quaternions. Although the quaternion has few advantages over Euler angle and direction cosine matrix representation, yet the inherent problem of unwinding [3], [26] due to the multiple equilibrium points are not addressed in the preceding papers. The phenomenon of unwinding if not undertaken while designing the control law, may cause the spacecraft to maneuver through the longest path instead of the nearest path for some initial conditions which leads to the wastage of fuel resources. In this paper, the spacecraft attitude is represented using three sets of variables by modified Rodrigues parameters (MRP), which provides the global representation (using shadow MRP) without facing the problem of unwinding. Whereas, the quaternion uses four sets of variables for global representation with an inherent problem of unwinding. Therefore, to the best of authors' knowledge, the study of robust event-triggered attitude regulation control of the flexible spacecraft using MRP under communication constraints has not yet been investigated. The main contributions of this work are stated below.

- 1) The robust event-triggered control is designed to achieve a satisfactory attitude regulation performance while compensating the effect of parametric uncertainties, external disturbances, and vibrations of flexible appendages under communication constraints.
- 2) The proposed controller uses only a single feedback vector for its update. Thus, it further helps in reducing the data transmission through the communication channel.
- 3) Moreover, the proposed event-triggered controller is free from Zeno behavior, i.e., it avoids the accumulation of triggering instants. This will guarantee the practical feasibility of the proposed scheme.
- 4) Finally, results obtained from comparative simulation study between the proposed event-triggered scheme, the periodically sampled data technique, and event-trigger based SMC technique [25] demonstrates the superiority of the proposed algorithm in the context of control over limited communication with less energy utilization.

The remaining part of this paper is organized as follows. In section II, the kinematic and dynamic equations of the flexible spacecraft subjected to multiple uncertainties and vibrations are modeled. In section III, a robust event-triggered attitude control is proposed. Then, the stability of the closed-loop system and the Zeno free behavior of the proposed control scheme are proved in section IV. In section V, multiple simulation results of the proposed scheme and its comparative analysis are reported. Finally, the paper is concluded in section VI.

## II. SYSTEM MODELING AND PROBLEM FORMULATION

In this paper, orientation of the flexible spacecraft is expressed in terms of MRP denoted by  $\mathbf{p} \in \mathbb{R}^3$ . The MRP can be written in terms of Euler axis as [27]

$$\mathbf{p} = \mathbf{e} \tan(\theta/4), \quad (1)$$

where  $\theta$  is the angle of rotation and  $\mathbf{e} = [e_1 \ e_2 \ e_3]^T \in \mathbb{R}^3$  is the Euler axis. It is obvious from (1) that  $\mathbf{p}$  goes to  $\infty$  when  $\theta = \pm 2\pi$ . The singularity of  $\mathbf{p}$  at  $\theta = \pm 2\pi$  has been solved using shadow MRP denoted by  $\mathbf{p}_s$  which is defined as [27]

$$\mathbf{p}_s = -\frac{\mathbf{p}}{\mathbf{p}^T \mathbf{p}} = \mathbf{e} \tan\left(\frac{\theta - 2\pi}{4}\right). \quad (2)$$

Although  $\mathbf{p}_s$  is nonsingular at  $\theta = \pm 2\pi$ , it also holds a singularity at  $\theta = 0$ . Therefore, a singularity-free attitude representation using MRP is obtained by switching between the normal MRP (1) and the shadow MRP (2) at the cost of discontinuity. The switching between the two parameter sets are governed according to the following rules [28]

$$\mathbf{p} = \begin{cases} \mathbf{p} & \text{if } \mathbf{p}^T \boldsymbol{\omega} \leq 0 \\ \mathbf{p}_s & \text{if } \mathbf{p}^T \boldsymbol{\omega} > 0, \end{cases} \quad (3)$$

where  $\boldsymbol{\omega} = [\omega_1, \omega_2, \omega_3]^T \in \mathbb{R}^3$  is the angular velocity vector. In the proposed work, it is considered that the switching is executed on the surface  $\|\mathbf{p}\| = \|\mathbf{p}_s\| = 1$ . With the help of these two MRP sets on the switching surface, the following unity constraint is obtained [28], [29]

$$\|\mathbf{p}\| \leq 1. \quad (4)$$

A beneficial property of  $\mathbf{p}_s$  is that it continues to follow the kinematic equations of spacecraft defined in (5) [28]. Moreover, with the use of two MRP sets, the time derivative of  $\mathbf{p}$  is globally defined except for the discontinuity at the switching boundary [28], [30].

### A. FLEXIBLE SPACECRAFT MODELING

The kinematic equations of the flexible spacecraft with respect to body-fixed frame are modeled as [31]:

$$\dot{\mathbf{p}} = \frac{1}{4}\{(1 - \mathbf{p}^T \mathbf{p})\mathbf{I} + 2\mathbf{p}^\times + 2\mathbf{p}\mathbf{p}^T\}\boldsymbol{\omega}, \quad (5)$$

where  $\mathbf{I}$  is the  $3 \times 3$  identity matrix, and the operator  $(\cdot)^\times$  is a skew symmetric matrix operator which is defined as:

$$\mathbf{p}^\times = \begin{bmatrix} 0 & -p_3 & p_2 \\ p_3 & 0 & -p_1 \\ -p_2 & p_1 & 0 \end{bmatrix}. \quad (6)$$

The dynamic equations of the flexible spacecraft are defined as follows [5], [32]:

$$J\dot{\boldsymbol{\omega}} + \delta^T \ddot{\boldsymbol{\eta}} = -\boldsymbol{\omega}^\times (J\boldsymbol{\omega} + \delta^T \dot{\boldsymbol{\eta}}) + \mathbf{u} + \mathbf{d}_0, \quad (7)$$

$$\ddot{\boldsymbol{\eta}} + C\dot{\boldsymbol{\eta}} = -K\boldsymbol{\eta} - \delta\dot{\boldsymbol{\omega}}, \quad (8)$$

where  $\mathbf{u} \in \mathbb{R}^3$  is the control input,  $\mathbf{d}_0 \in \mathbb{R}^3$  is the external disturbance,  $J \in \mathbb{R}^{3 \times 3}$  is the symmetric inertia matrix of the

spacecraft,  $\boldsymbol{\eta} \in \mathbb{R}^n$  represents the  $n$  number of modal coordinate vector of the flexible appendages, and  $\delta \in \mathbb{R}^{n \times 3}$  is a constant matrix which represents the coupling effect between the flexible and rigid structures. As considered in [5], in this work also  $\boldsymbol{\eta}$  is considered to have four modal components, i.e.,  $\boldsymbol{\eta} = [\eta_1, \eta_2, \eta_3, \eta_4]^T \in \mathbb{R}^4$ , and  $\delta \in \mathbb{R}^{4 \times 3}$ . The damping and stiffness matrices are represented by  $C \in \mathbb{R}^{4 \times 4}$  and  $K \in \mathbb{R}^{4 \times 4}$ , respectively which are expressed as:

$$C = \begin{bmatrix} 2\zeta_1 w_1 & \cdots & 0 \\ \vdots & \ddots & \vdots \\ 0 & \cdots & 2\zeta_4 w_4 \end{bmatrix} \quad K = \begin{bmatrix} w_1^2 & \cdots & 0 \\ \vdots & \ddots & \vdots \\ 0 & \cdots & w_4^2 \end{bmatrix}, \quad (9)$$

where  $w_i$  and  $\zeta_i$  are the natural frequency and the damping ratio of  $i^{\text{th}}$  order elastic mode, respectively for  $i = 1, 2, 3, 4$ .

Now, defining a new auxiliary variable  $\boldsymbol{\varpi} \in \mathbb{R}^4$  as

$$\boldsymbol{\varpi} = \delta\boldsymbol{\omega} + \dot{\boldsymbol{\eta}}. \quad (10)$$

The time derivative of  $\boldsymbol{\varpi}$  can be expressed by using  $\ddot{\boldsymbol{\eta}}$  from (8) and  $\dot{\boldsymbol{\eta}}$  from (10) as

$$\dot{\boldsymbol{\varpi}} = \delta\dot{\boldsymbol{\omega}} + \ddot{\boldsymbol{\eta}}, \quad (11)$$

$$= -C\dot{\boldsymbol{\eta}} - K\boldsymbol{\eta} = -C\boldsymbol{\varpi} + C\delta\boldsymbol{\omega} - K\boldsymbol{\eta}. \quad (12)$$

From (11) and (12), it can be written as

$$\delta\dot{\boldsymbol{\omega}} + \ddot{\boldsymbol{\eta}} = -C\boldsymbol{\varpi} + C\delta\boldsymbol{\omega} - K\boldsymbol{\eta}. \quad (13)$$

Multiplying  $\delta^T$  on both side of (13) and then rearranging the terms yield

$$\delta^T \ddot{\boldsymbol{\eta}} = -\delta^T \delta\dot{\boldsymbol{\omega}} - \delta^T C\boldsymbol{\varpi} + \delta^T C\delta\boldsymbol{\omega} - \delta^T K\boldsymbol{\eta}. \quad (14)$$

Substituting  $\delta^T \ddot{\boldsymbol{\eta}}$  from (14) into the dynamical equation (7) yields

$$(J - \delta^T \delta)\dot{\boldsymbol{\omega}} = \delta^T C\boldsymbol{\varpi} + \delta^T K\boldsymbol{\eta} - \delta^T C\delta\boldsymbol{\omega} - \boldsymbol{\omega}^\times J\boldsymbol{\omega} - \boldsymbol{\omega}^\times \delta^T (\boldsymbol{\varpi} - \delta\boldsymbol{\omega}) + \mathbf{u} + \mathbf{d}_0. \quad (15)$$

Considering a lumped perturbation variable  $\boldsymbol{\psi} \in \mathbb{R}^3$  in (15) which involves the coupling effect and rewriting it as

$$(J - \delta^T \delta)\dot{\boldsymbol{\omega}} = -\boldsymbol{\omega}^\times J\boldsymbol{\omega} + \boldsymbol{\psi} + \mathbf{u} + \mathbf{d}_0, \quad (16)$$

where

$$\boldsymbol{\psi} = \delta^T [K \quad C] \begin{bmatrix} \boldsymbol{\eta} \\ \boldsymbol{\varpi} \end{bmatrix} - \delta^T C\delta\boldsymbol{\omega} - \boldsymbol{\omega}^\times \delta^T (\boldsymbol{\varpi} - \delta\boldsymbol{\omega}). \quad (17)$$

The spacecraft undergoes various operations like fuel consumption, onboard solar arrays rotation, payload motion, and out-gassing, etc. which leads to mass variations [33]. Therefore, the inertia matrix  $J$  consists of a nominal component  $J_0 \in \mathbb{R}^{3 \times 3}$  and an uncertain component  $\Delta J \in \mathbb{R}^{3 \times 3}$ . The uncertain term  $\Delta J$  can also be written as  $\Delta J = J - J_0$  [34].

Now rearranging all the uncertainties as a single lumped uncertainty in (16) as

$$\underbrace{(J_0 - \delta^T \delta)}_{J_0} \dot{\boldsymbol{\omega}} = -\boldsymbol{\omega}^\times (J_0 + \Delta J)\boldsymbol{\omega} + \boldsymbol{\psi} + \mathbf{u} + \mathbf{d}_0.$$

For the stabilizing control law  $\mathbf{u}$ , one needs to design the system such that  $\mathcal{J}_0 > 0 \in \mathbb{R}^{3 \times 3}$ . Therefore,

$$(\mathcal{J}_0 + \Delta J)\dot{\boldsymbol{\omega}} = -\boldsymbol{\omega}^\times \mathcal{J}_0 \boldsymbol{\omega} - \boldsymbol{\omega}^\times \Delta J \boldsymbol{\omega} + \boldsymbol{\psi} + \mathbf{u} + \mathbf{d}_0. \quad (18)$$

Taking the inverse of  $(\mathcal{J}_0 + \Delta J)$  in (18)

$$\dot{\boldsymbol{\omega}} = (\mathcal{J}_0 + \Delta J)^{-1} \{-\boldsymbol{\omega}^\times \mathcal{J}_0 \boldsymbol{\omega} - \boldsymbol{\omega}^\times \Delta J \boldsymbol{\omega} + \boldsymbol{\psi} + \mathbf{u} + \mathbf{d}_0\}. \quad (19)$$

The inverse of  $(\mathcal{J}_0 + \Delta J)$  can be written as [35]

$$(\mathcal{J}_0 + \Delta J)^{-1} = \mathcal{J}_0^{-1} + \Delta \hat{J}, \quad (20)$$

where  $\Delta \hat{J} = -\mathcal{J}_0^{-1} \Delta J (\mathcal{I}_{3 \times 3} + \mathcal{J}_0^{-1} \Delta J)^{-1} \mathcal{J}_0^{-1}$ . Using (20), the equation (19) can be rewritten as:

$$\begin{aligned} \dot{\boldsymbol{\omega}} &= \mathcal{J}_0^{-1} \{-\boldsymbol{\omega}^\times \mathcal{J}_0 \boldsymbol{\omega} - \boldsymbol{\omega}^\times \Delta J \boldsymbol{\omega} + \boldsymbol{\psi} + \mathbf{u} + \mathbf{d}_0\} \\ &+ \Delta \hat{J} \{-\boldsymbol{\omega}^\times \mathcal{J}_0 \boldsymbol{\omega} - \boldsymbol{\omega}^\times \Delta J \boldsymbol{\omega} + \boldsymbol{\psi} + \mathbf{u} + \mathbf{d}_0\}. \end{aligned} \quad (21)$$

The equation (21) can further be simplified by combining all the uncertainty terms in a single term  $\mathbf{d}$  as:

$$\dot{\boldsymbol{\omega}} = -\mathcal{J}_0^{-1} \boldsymbol{\omega}^\times \mathcal{J}_0 \boldsymbol{\omega} + \mathcal{J}_0^{-1} \mathbf{u} + \mathcal{J}_0^{-1} \mathbf{d}, \quad (22)$$

where  $\mathbf{d} \in \mathbb{R}^3$  represents the total disturbance which comprises of inertial uncertainties, external disturbances, and flexible vibrations. The expression of  $\mathbf{d}$  is given as:

$$\begin{aligned} \mathbf{d} &= -\boldsymbol{\omega}^\times \Delta J \boldsymbol{\omega} + (\mathcal{I}_{3 \times 3} + \mathcal{J}_0 \Delta \hat{J}) \boldsymbol{\psi} - \mathcal{J}_0 \Delta \hat{J} \boldsymbol{\omega}^\times (\mathcal{J}_0 + \Delta J) \\ &\times \boldsymbol{\omega} + \mathcal{J}_0 \Delta \hat{J} \mathbf{u} + (\mathcal{I}_{3 \times 3} + \mathcal{J}_0 \Delta \hat{J}) \mathbf{d}_0. \end{aligned} \quad (23)$$

Therefore, the complete attitude kinematics and dynamics of the flexible spacecraft are governed by (5) and (22).

### B. PROBLEM STATEMENT

The objective of this work is to regulate the attitude of the flexible spacecraft to a set point under limited utilization of control updating frequency. This means less number of transmission of feedback information. Moreover, the proposed controller is also required to compensate for the effects of parametric uncertainties, external disturbances, and vibrations due to flexible appendages. The problem statement can be summarized as, design a robust event-triggered control under communication constraints for the flexible spacecraft model (5) and (22) so that the closed loop system trajectories converge into a small bound near the neighborhood of origin, i.e.,

$$\lim_{t \rightarrow \infty} \mathbf{p} = [0, 0, 0]^T, \text{ and } \lim_{t \rightarrow \infty} \boldsymbol{\omega} = [0, 0, 0]^T. \quad (24)$$

### III. CONTROL METHODOLOGY AND DESIGN STRUCTURE

Before discussing the proposed controller, let's briefly describe the primary difference between the traditional periodically sampled data approach and the event-triggered approach. In a periodically sampled data technique, the time of sampling is constant, i.e., computation and update of the control input data are at a fixed sample time. The periodic sample time is determined as  $T = t_{i+1} - t_i$ , where  $T > 0$ , and  $t_i$  is the  $i^{\text{th}}$  time of triggering (or sampling) instant for  $i = 0, 1, 2, \dots$ . So, the execution of controller input is carried out at every  $T$  interval. In contrast, the sampling time in

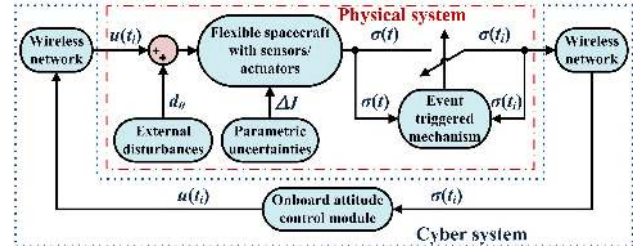


FIGURE 2. Proposed robust event-driven attitude control system structure.

the event-trigger technique is not constant, and it is termed as inter-update time,  $T_i = t_{i+1} - t_i$ . So, the control signal herein is updated at every triggering instant which is decided by a specific predefined triggering condition. The value of  $\mathbf{u}(t)$  between the two triggering instant is kept constant for time  $T_i$ . Therefore, the control law will update whenever there is a requirement for the change in the control input. Thus, the aperiodic update will significantly reduce the burden on the communication network.

### A. PROPOSED EVENT-TRIGGERED CONTROL LAW

The basic schematic representation of the proposed control scheme is depicted in Fig. 2. As seen in Fig. 2, the overall system is divided into two parts, physical system, and cyber system. The physical system comprises of the physical plant, sensors, and physical measurements, whereas the cyber system transmits the feedback data of the system states through the communication channel.

The feedback vector  $\boldsymbol{\sigma}$  is defined as:

$$\boldsymbol{\sigma} = \boldsymbol{\omega} + \alpha \mathbf{p} + \alpha (\mathbf{p}^T \mathbf{p}) \mathbf{p}, \quad (25)$$

where  $\boldsymbol{\sigma} = [\sigma_1 \ \sigma_2 \ \sigma_3]^T \in \mathbb{R}^3$ ,  $\alpha > 0$  is a constant which is to be designed.

The proposed robust event-triggered attitude control law is developed using the event-triggered feedback vector  $\boldsymbol{\sigma}(t_i)$  as:

$$\mathbf{u}(t) = -k \boldsymbol{\sigma}(t_i), \quad \text{for } t \in [t_i, t_{i+1}), i = 0, 1, \dots \quad (26)$$

where  $k > 0$  is a gain constant which needs to be designed. The value of control input  $\mathbf{u}(t)$  is kept constant between every two consecutive triggering instants, i.e.,  $t_i$  and  $t_{i+1}$ .

An additional benefit of the designed controller is its ability to regulate the attitude of flexible spacecraft using a single feedback vector  $\boldsymbol{\sigma}(t_i)$ . Thus, it helps in easing the burden of communication resources by transmitting a single vector for the update of the control input to the actuator module. On the contrary, the update of the control input in the existing literature is often required to have the individual information of  $\mathbf{p}$  and  $\boldsymbol{\omega}$  through the communication network.

### B. THE WORKING OF THE PROPOSED SCHEME

The triggering instants of the proposed controller (26) significantly depend upon the measurement error which is defined as:

$$\boldsymbol{\Xi} = \boldsymbol{\sigma}(t_i) - \boldsymbol{\sigma}, \quad t \in [t_i, t_{i+1}), \quad (27)$$

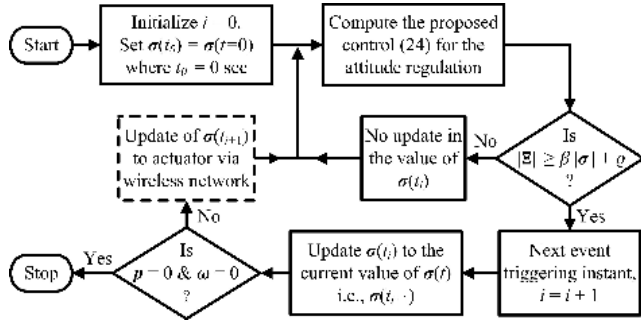


**FIGURE 3.** Flowchart of the proposed robust event-triggered control scheme.

where  $\Xi = [\Xi_1 \ \Xi_2 \ \Xi_3]^T \in \mathbb{R}^3$ . The increment of  $\Xi$  is closely monitored approximately in a continuous way. So, the next triggering instant  $t_{i+1}$  occurs when  $\Xi$  crosses the threshold of a predefined state-dependent condition which is defined as

$$t_{i+1} = \min[t \geq t_i : \|\Xi\| \geq \beta \|\sigma\| + \varrho], \quad i = 0, 1, 2, \dots \quad (28)$$

where  $\varrho > 0$  &  $\beta \in (0, 1)$ . The parameter  $\varrho$  is incorporated to avoid Zeno behavior, as explained in the next section.

The general working of the proposed scheme to the flexible spacecraft regulation problem is demonstrated with the help of the flowchart given in Fig. 3.

**Remark 1:** The inter-update time  $T_i$  is dependent on the value of  $\beta$ . The parameter  $\beta$  is directly proportional to  $T_i$ . So, a higher value of  $\beta$  will generate larger  $T_i$ , which means less number of data transmission, but at the same time, it will produce higher steady-state attitude control errors. Therefore, while designing the value of  $\beta$ , an acceptable trade-off between the steady-state errors and the communication burden needs to be established. Thus, a suitable value of  $\beta$  will put less stress on the transmission network while achieving better steady-state performance.

Some of the necessary properties and assumptions which are essential for the controller design are stated in the subsequent development.

**Property 1 ([3]):** Any symmetric positive-definite matrix  $J$  satisfies the condition (29) for any vector  $v = [v_1 \ v_2 \ v_3]^T \in \mathbb{R}^3$ :

$$\lambda_{\min}(J) \|v\|^2 \leq v^T J v \leq \lambda_{\max}(J) \|v\|^2, \quad (29)$$

where  $\lambda_{\max}(J)$  and  $\lambda_{\min}(J)$  are the maximum and minimum eigenvalues of  $J$ , respectively.

Throughout this paper, the following assumptions are considered.

**Assumption 1:** The coupling effect variable  $\psi$  defined in (17) is considered as a lumped perturbation and assumed to be bounded as it is considered in [7], [32], [36], [37]. The bound on  $\psi(t)$  satisfies  $\|\psi(t)\| \leq r_1 + r_2 \|\omega\|^2$  where  $r_1 > 0$  and  $r_2 > 0$ . The bound can also be expressed as  $\|\psi(t)\| \leq r \Delta$  where  $\Delta = 1 + \|\omega\|^2$  and  $r = \max(r_1, r_2)$  [33].

**Assumption 2:** The overall disturbance  $d$  in (23) is assumed to be bounded, i.e.,  $\|d\| \leq \bar{d}$  where  $\bar{d} > 0$  represents the upper bound of  $d$ .

**Assumption 3:** The measurements of MRP and angular velocity are accessible for the feedback control.

**Remark 2:** Generally, the sources which emanate the disturbances in the spacecraft are from aerodynamic drag, magnetic forces, pressure due to solar radiation, gravitation, etc. All these sources of disturbances are assumed bounded [36].

**Remark 3:** In this paper, the actuator dynamics is considered to be faster than the plant dynamics. This implies that the time constants of the actuators are very small. Therefore, the actuator dynamics can be ignored in designing the controller [38].

#### IV. STABILITY ANALYSIS AND THE FEASIBILITY OF THE PROPOSED CONTROLLER

In this section, two theorems are proposed. Theorem 1 demonstrates the stability analysis of the closed-loop system and the theorem 2 shows the Zeno free behavior in the proposed scheme.

**Theorem 1:** Consider the flexible spacecraft dynamics (5), (22) under the assumption 1 and 2, with the event triggering condition (28). Then the proposed event-triggered control law (26) will guarantee that the closed-loop system trajectories  $p$  and  $\omega$  are uniformly ultimately bounded (UUB), and hence resides within a small set in the vicinity of the origin defined by  $\lim_{t \rightarrow \infty} \|\omega(t)\| \in \mathcal{U}_\omega$  and  $\lim_{t \rightarrow \infty} \|p(t)\| \in \mathcal{U}_p$ , where  $\mathcal{U}_\omega$  and  $\mathcal{U}_p$  are expressed as

$$\mathcal{U}_\omega = \left\{ \omega \mid \|\omega\| \leq \sqrt{\frac{2\Phi}{\lambda_{\min}(\mathcal{J}_0)\varsigma}} \right\}, \quad (30)$$

$$\mathcal{U}_p = \left\{ p \mid \|p\| \leq \sqrt{\frac{\Phi}{k\alpha\varsigma}} \right\}, \quad (31)$$

where  $\varsigma$  and  $\Phi$  are positive constants which are defined as

$$\varsigma = \frac{2[k(1-\beta) - v]}{\lambda_{\max}(\mathcal{J}_0)}, \quad (32)$$

$$\Phi = \frac{4k\alpha[k(1-\beta) - v]}{\lambda_{\max}(\mathcal{J}_0)} + \frac{(k\varrho + 2k\alpha\beta + \bar{d})^2}{4v}. \quad (33)$$

**Proof:** Consider a positive Lyapunov function

$$V = 2k\alpha p^T p + \frac{1}{2} \omega^T \mathcal{J}_0 \omega. \quad (34)$$

Substituting (5) and (22) in the time derivative of (34) yields

$$\begin{aligned} \dot{V} &= 4k\alpha p^T \dot{p} + \omega^T \mathcal{J}_0 \dot{\omega}, \\ &= 4k\alpha p^T \frac{1}{4} \{(1 - p^T p)I + 2p^\times + 2pp^T\} \omega \\ &\quad + \omega^T (-\omega^\times \mathcal{J}_0 \omega + u + d). \end{aligned} \quad (35)$$

Applying the property of skew symmetric matrix, i.e.,  $\omega^T \omega^\times = 0$  or  $p^T p^\times = 0$  [3], results

$$\dot{V} = k\alpha \{p^T \omega + p^T p p^T \omega\} + \omega^T u + \omega^T d. \quad (37)$$

Substituting the control input (26) into (37)

$$\dot{V} = k\alpha \{p^T \omega + p^T p p^T \omega\} - k\omega^T \sigma(t_i) + \omega^T d. \quad (38)$$

From (25) and (27),  $\dot{V}$  can be expressed as

$$\begin{aligned}\dot{V} &= k\alpha\{\mathbf{p}^T\boldsymbol{\omega} + \mathbf{p}^T\mathbf{p}\mathbf{p}^T\boldsymbol{\omega}\} - k\boldsymbol{\omega}^T(\boldsymbol{\Xi} + \boldsymbol{\sigma}) + \boldsymbol{\omega}^T\mathbf{d}, \\ &= k\alpha\{\mathbf{p}^T\boldsymbol{\omega} + (\mathbf{p}^T\mathbf{p})\mathbf{p}^T\boldsymbol{\omega}\} - k\boldsymbol{\omega}^T\{\boldsymbol{\Xi} + \boldsymbol{\omega} + \alpha\mathbf{p} \\ &\quad + \alpha(\mathbf{p}^T\mathbf{p})\mathbf{p}\} + \boldsymbol{\omega}^T\mathbf{d}, \\ &= -k\boldsymbol{\omega}^T\boldsymbol{\omega} - k\boldsymbol{\omega}^T\boldsymbol{\Xi} + \boldsymbol{\omega}^T\mathbf{d}, \\ &\leq -k\|\boldsymbol{\omega}\|^2 + k\|\boldsymbol{\omega}\|\|\boldsymbol{\Xi}\| + \bar{d}\|\boldsymbol{\omega}\|. \end{aligned} \quad (39)$$

The triggering condition (28) is used in (39) to get

$$\dot{V} \leq -k\|\boldsymbol{\omega}\|^2 + k\|\boldsymbol{\omega}\|(\beta\|\boldsymbol{\sigma}\| + \varrho) + \bar{d}\|\boldsymbol{\omega}\|. \quad (40)$$

With the help of the unity constraint (4),  $\|\boldsymbol{\sigma}\|$  can further be simplified as

$$\begin{aligned}\|\boldsymbol{\sigma}\| &= \|\boldsymbol{\omega} + \alpha\mathbf{p} + \alpha(\mathbf{p}^T\mathbf{p})\mathbf{p}\|, \\ &\leq \|\boldsymbol{\omega}\| + \|\alpha\mathbf{p}\| + \|\alpha(\mathbf{p}^T\mathbf{p})\mathbf{p}\|, \\ &\leq \|\boldsymbol{\omega}\| + 2\alpha. \end{aligned} \quad (41)$$

Substituting (41) into (40) gives

$$\begin{aligned}\dot{V} &\leq -k\|\boldsymbol{\omega}\|^2 + k\|\boldsymbol{\omega}\|\{\beta(\|\boldsymbol{\omega}\| + 2\alpha) + \varrho\} + \bar{d}\|\boldsymbol{\omega}\|, \\ &= -k(1 - \beta)\|\boldsymbol{\omega}\|^2 + (k\varrho + 2k\alpha\beta + \bar{d})\|\boldsymbol{\omega}\|. \end{aligned} \quad (42)$$

Now, adding and subtracting a positive term  $\nu\|\boldsymbol{\omega}\|^2$  in (42), such that  $0 < \nu < k(1 - \beta)$

$$\begin{aligned}\dot{V} &\leq -k(1 - \beta)\|\boldsymbol{\omega}\|^2 + \nu\|\boldsymbol{\omega}\|^2 + (k\varrho + 2k\alpha\beta + \bar{d})\|\boldsymbol{\omega}\| \\ &\quad + \frac{(k\varrho + 2k\alpha\beta + \bar{d})^2}{4\nu} - \frac{(k\varrho + 2k\alpha\beta + \bar{d})^2}{4\nu} - \nu\|\boldsymbol{\omega}\|^2, \\ &= -[k(1 - \beta) - \nu]\|\boldsymbol{\omega}\|^2 + \frac{(k\varrho + 2k\alpha\beta + \bar{d})^2}{4\nu} - \{\nu\|\boldsymbol{\omega}\|^2 \\ &\quad - (k\varrho + 2k\alpha\beta + \bar{d})\|\boldsymbol{\omega}\| + \frac{(k\varrho + 2k\alpha\beta + \bar{d})^2}{4\nu}\}, \\ &= -[k(1 - \beta) - \nu]\|\boldsymbol{\omega}\|^2 + \frac{(k\varrho + 2k\alpha\beta + \bar{d})^2}{4\nu} \\ &\quad - \left\{\sqrt{\nu}\|\boldsymbol{\omega}\| - \frac{(k\varrho + 2k\alpha\beta + \bar{d})}{2\sqrt{\nu}}\right\}^2, \\ &\leq -[k(1 - \beta) - \nu]\|\boldsymbol{\omega}\|^2 + \frac{(k\varrho + 2k\alpha\beta + \bar{d})^2}{4\nu}. \end{aligned} \quad (43)$$

Using the Property 1 to express  $\|\boldsymbol{\omega}\|^2$  as

$$\|\boldsymbol{\omega}\|^2 \geq \frac{1}{\lambda_{\max}(\mathcal{J}_0)}\boldsymbol{\omega}^T\mathcal{J}_0\boldsymbol{\omega}. \quad (44)$$

Applying (44) into (43) and rewriting it as

$$\begin{aligned}\dot{V} &\leq -\frac{2[k(1 - \beta) - \nu]}{\lambda_{\max}(\mathcal{J}_0)}\left(\frac{1}{2}\boldsymbol{\omega}^T\mathcal{J}_0\boldsymbol{\omega}\right) + \frac{(k\varrho + 2k\alpha\beta + \bar{d})^2}{4\nu} \\ &\quad + \frac{2[k(1 - \beta) - \nu]}{\lambda_{\max}(\mathcal{J}_0)}\left\{2k\alpha\mathbf{p}^T\mathbf{p}\right\} - \frac{2[k(1 - \beta) - \nu]}{\lambda_{\max}(\mathcal{J}_0)} \\ &\quad \times \left\{2k\alpha\mathbf{p}^T\mathbf{p}\right\}, \\ &= -\frac{2[k(1 - \beta) - \nu]}{\lambda_{\max}(\mathcal{J}_0)}\underbrace{\left\{\frac{1}{2}\boldsymbol{\omega}^T\mathcal{J}_0\boldsymbol{\omega} + 2k\alpha\mathbf{p}^T\mathbf{p}\right\}}_V \end{aligned} \quad (45)$$

$$+ \frac{2[k(1 - \beta) - \nu]}{\lambda_{\max}(\mathcal{J}_0)}\left\{2k\alpha\mathbf{p}^T\mathbf{p}\right\} + \frac{(k\varrho + 2k\alpha\beta + \bar{d})^2}{4\nu}. \quad (46)$$

Further taking the upper bound of (46) yields

$$\begin{aligned}\dot{V} &\leq -\frac{2[k(1 - \beta) - \nu]}{\lambda_{\max}(\mathcal{J}_0)}V + \frac{4k\alpha[k(1 - \beta) - \nu]}{\lambda_{\max}(\mathcal{J}_0)}\|\mathbf{p}^T\mathbf{p}\| \\ &\quad + \frac{(k\varrho + 2k\alpha\beta + \bar{d})^2}{4\nu}, \end{aligned} \quad (47)$$

$$\begin{aligned}\dot{V} &\leq -\frac{2[k(1 - \beta) - \nu]}{\lambda_{\max}(\mathcal{J}_0)}V + \frac{4k\alpha[k(1 - \beta) - \nu]}{\lambda_{\max}(\mathcal{J}_0)} \\ &\quad + \frac{(k\varrho + 2k\alpha\beta + \bar{d})^2}{4\nu}, \end{aligned} \quad (48)$$

$$\dot{V} \leq -\varsigma V + \Phi, \quad (49)$$

where

$$\varsigma = \frac{2[k(1 - \beta) - \nu]}{\lambda_{\max}(\mathcal{J}_0)} > 0, \quad (50)$$

$$\Phi = \frac{4k\alpha[k(1 - \beta) - \nu]}{\lambda_{\max}(\mathcal{J}_0)} + \frac{(k\varrho + 2k\alpha\beta + \bar{d})^2}{4\nu} > 0, \quad (51)$$

and  $\lambda_{\max}(\mathcal{J}_0) > 0$  is the maximum eigenvalue of the positive definite matrix  $\mathcal{J}_0$ .

From the solution of (49), the largest invariant set in which the trajectories of the closed loop system resides can be defined as

$$\Psi = \left\{(\mathbf{p}, \boldsymbol{\omega}) \mid V(\mathbf{p}, \boldsymbol{\omega}) \leq \frac{\Phi}{\varsigma}\right\}. \quad (52)$$

With assumption 1 and 2 under a high gain controller, the bound  $\Phi$  can be narrowed down to a small bound in the vicinity of zero. So, the largest invariant band  $\Psi$  will also be narrowed down to a smaller set near the neighborhood of zero. Therefore, the Lyapunov function  $V$  will ultimately resides in the small set  $\Psi$  in the vicinity of origin. Whereas, the closed loop system states ultimately converges within the following ultimate bounds:

$$\|\mathbf{p}\| \leq \sqrt{\frac{\Phi}{k\alpha\varsigma}} = \sqrt{\frac{\Psi}{k\alpha}}, \quad (53)$$

$$\|\boldsymbol{\omega}\| \leq \sqrt{\frac{2\Phi}{\lambda_{\min}(\mathcal{J}_0)\varsigma}} = \sqrt{\frac{2\Psi}{\lambda_{\min}(\mathcal{J}_0)}}. \quad (54)$$

Thus, the overall closed loop system will remain uniformly ultimately bounded (UUB). This completes the proof of theorem 1.  $\square$

As mentioned in the previous section, the event-triggered technique involves the use of consecutive triggering sequence  $t_i$  for  $i = 0, 1, 2, \dots$ . So, it might face a situation where the accumulation of triggering instants occur, which is called a Zeno behavior. The practical applicability of the continuous attitude controller depends upon the admissibility of the triggering sequence. Therefore, it is necessary that the event-triggered attitude controller must be free from Zeno behavior. The condition, i.e., ‘the inter-update time  $T_i$  of the controller must always be lower bounded by a positive value’

will guarantee the nonexistence of Zeno behavior [39]. Thus, the practical feasibility of the triggering sequence depends upon consistently positive  $T_i$ .

The following comparison lemma is used in the proof of theorem 2.

**Lemma 1 ([40]):** Suppose  $\dot{x} = g(t, x)$ ,  $x(t_0) = x_0$ , where  $g(t, x)$  is continuous in  $t$  and locally Lipschitz in  $x$ ,  $\forall t \geq 0$  and  $\forall x \in J \subset \mathbb{R}$ . Let  $[t_0, T)$  ( $T$  can be  $\infty$ ) be the maximal interval of existence of the solution  $x(t) \in J \forall t \in [t_0, T)$ . Let  $\vartheta(t)$  be a continuous function whose upper right-hand derivative  $D^+\vartheta(t)$  satisfies the following differential inequality

$$D^+\vartheta(t) \leq g(t, \vartheta(t)), \quad \vartheta(t_0) \leq x_0, \quad (55)$$

with  $\vartheta(t) \in J \forall t \in [t_0, T)$ . Then  $\vartheta(t) \leq x(t) \forall t \in [t_0, T)$ .

**Theorem 2:** While considering the assumption 1 & 2, the flexible spacecraft dynamics (5) and (22) with the proposed event-triggered control scheme (26), the event triggering rule (28) guarantees that the inter-update time  $T_i$  is always lower bounded by a positive value apart from the origin.

**Proof:** Under the proposed scheme, the inter-update time  $T_i$  at a particular triggering instant is defined as the time taken by  $\|\Xi\|$  to ascent from 0 to  $\beta\|\sigma\| + \varrho$ . The inter-update time at the  $(i+1)^{\text{th}}$  time instant is defined as  $T_i = t_{i+1} - t_i$ . Now, defining  $\Theta$  as a time instant where  $\Theta := \{t \in [t_i, t_{i+1}) : \|\Xi(t)\| = 0\}$ . So, for  $t \in [t_i, t_{i+1}) \setminus \Theta$ , the derivative of  $\|\Xi(t)\|$  with respect to time is defined as

$$\begin{aligned} \frac{d}{dt} \|\Xi(t)\| &\leq \left\| \frac{d}{dt} [\sigma(t_i) - \sigma(t)] \right\|, \\ &= \left\| \frac{d}{dt} \sigma(t) \right\|. \end{aligned} \quad (56)$$

Using  $\dot{p}$  from (5) and  $\dot{\omega}$  from (22), the time derivative of  $\mathcal{J}_0\sigma$  from (25) can be expressed as

$$\begin{aligned} \mathcal{J}_0\dot{\sigma} &= \mathcal{J}_0\dot{\omega} + \alpha\mathcal{J}_0\dot{p} + 2\alpha\mathcal{J}_0(p^T\dot{p})p + \alpha\mathcal{J}_0(p^Tp)\dot{p}, \\ \mathcal{J}_0\dot{\sigma} &= \mathcal{J}_0\dot{\omega} + \alpha(1 + p^Tp)\mathcal{J}_0\dot{p} + 2\alpha\mathcal{J}_0(p^T\dot{p})p, \\ \mathcal{J}_0\dot{\sigma} &= -\omega^\times J_0\omega + u + d + \frac{\alpha(1 + p^Tp)}{4}\mathcal{J}_0\{(1 - p^Tp)I \\ &\quad + 2p^\times + 2pp^T\}\omega + \frac{2}{4}\alpha\mathcal{J}_0\{p^T[(1 - p^Tp)I + 2p^\times \\ &\quad + 2pp^T]\omega\}p. \end{aligned} \quad (57)$$

Further simplifying the equation (57) yields

$$\begin{aligned} \mathcal{J}_0\dot{\sigma} &= -\omega^\times J_0\omega + u + d + \frac{\alpha\mathcal{J}_0}{4}\{1 - (p^Tp)^2\}I\omega \\ &\quad + \frac{\alpha\mathcal{J}_0}{4}(1 - p^Tp)(2p^\times + 2pp^T)\omega + \frac{\alpha\mathcal{J}_0}{2}\{p^TI \\ &\quad + p^Tpp^T\}\omega\}p. \end{aligned} \quad (58)$$

Defining a new variable  $\mathcal{G}(\cdot)$  as

$$\begin{aligned} \mathcal{G}(\cdot) &= -\omega^\times J_0\omega + d + \frac{\alpha\mathcal{J}_0}{4}\{1 - (p^Tp)^2\}I\omega \\ &\quad + \frac{\alpha\mathcal{J}_0}{4}(1 - p^Tp)(2p^\times + 2pp^T)\omega + \frac{\alpha\mathcal{J}_0}{2}\{p^TI \\ &\quad + p^Tpp^T\}\omega\}p. \end{aligned} \quad (59)$$

The upper bound of  $\mathcal{G}(\cdot)$  using unity constraint (4) can be expressed as

$$\begin{aligned} \|\mathcal{G}(\cdot)\| &= \underbrace{\|-\omega^\times J_0\omega\|}_{\leq c_1\|\omega\|^2} + \underbrace{\left\|\frac{\alpha\mathcal{J}_0}{4}\{1 - (p^Tp)^2\}I\omega\right\|}_{\leq c_2\|\omega\|} \\ &\quad + \underbrace{\left\|\frac{\alpha\mathcal{J}_0}{4}(1 - p^Tp)(2p^\times + 2pp^T)\omega\right\|}_{\leq c_3\|\omega\|} + \|d\| \\ &\quad + \underbrace{\left\|\frac{\alpha\mathcal{J}_0}{2}\{p^TI + p^Tpp^T\}\omega\}p\right\|}_{\leq c_4\|\omega\|}, \end{aligned} \quad (60)$$

$$\leq c_1\|\omega\|^2 + c_2\|\omega\| + c_3\|\omega\| + c_4\|\omega\| + \bar{d}, \quad (61)$$

$$= c_1\|\omega\|^2 + c_{24}\|\omega\| + \bar{d}, \quad (62)$$

$$\leq \max\{c_1, c_{24}, \bar{d}\}(\|\omega\|^2 + \|\omega\| + 1), \quad (63)$$

$$\|\mathcal{G}(\cdot)\| \leq \Gamma\Omega, \quad (64)$$

where  $\Gamma = \max\{c_1, c_{24}, \bar{d}\} > 0$ ,  $\Omega = \|\omega\|^2 + \|\omega\| + 1$ ,  $c_{24} = c_2 + c_3 + c_4$ , and  $c_i > 0$  for  $i = 1, 2, 3, 4$ .

Therefore, the equation (58) can be rewritten as

$$\begin{aligned} \mathcal{J}_0\dot{\sigma} &= \mathcal{G}(\cdot) + u, \\ \text{or, } \dot{\sigma} &= \mathcal{J}_0^{-1}[\mathcal{G}(\cdot) + u]. \end{aligned} \quad (65)$$

Substituting  $\dot{\sigma}$  from (65) into (56) results in

$$\frac{d}{dt} \|\Xi(t)\| \leq \|\mathcal{J}_0^{-1}\| \|\mathcal{G}(\cdot) + u\|. \quad (66)$$

The control input  $u$  from (26) is substituted into (66) to yield

$$\begin{aligned} \frac{d}{dt} \|\Xi(t)\| &\leq \|\mathcal{J}_0^{-1}\| \|\mathcal{G}(\cdot) - k\sigma(t_i)\|, \\ &\leq \|\mathcal{J}_0^{-1}\| \|\mathcal{G}(\cdot)\| + \|\mathcal{J}_0^{-1}\| \|k\sigma + k\Xi\|, \\ &\leq \|\mathcal{J}_0^{-1}\| \Gamma\Omega + k \|\mathcal{J}_0^{-1}\| \|\sigma\| + k \|\mathcal{J}_0^{-1}\| \|\Xi\|. \end{aligned} \quad (67)$$

The comparison lemma from [40] (Lemma 1) is employed to obtain the solution of (67) with  $\|\Xi(t)\| = 0$  as the initial condition. Therefore, the solution of  $\|\Xi(t)\|$  is expressed as

$$\|\Xi(t)\| \leq \frac{\Gamma\Omega + k\|\sigma(t_i)\|}{k} [\exp\{k \|\mathcal{J}_0^{-1}\| (t - t_i)\} - 1]. \quad (68)$$

The occurrence of next triggering instance at  $t_{i+1}$  time can be visualized mathematically using the triggering condition (28) and the expression of  $\|\Xi(t_{i+1})\|$  from (68) as

$$\beta\|\sigma(t_{i+1})\| + \varrho = \|\Xi(t_{i+1})\|, \quad (69)$$

$$\leq \frac{\Gamma\Omega + k\|\sigma(t_{i+1})\|}{k} [\exp\{k \|\mathcal{J}_0^{-1}\| T_i\} - 1]. \quad (70)$$

Rearranging (70) to obtain the lower bound by  $T_i$  as

$$T_i \geq \frac{1}{k \|\mathcal{J}_0^{-1}\|} \ln \left\{ 1 + \frac{k \|\Xi(t_{i+1})\|}{\Gamma\Omega + k\|\sigma(t_{i+1})\|} \right\}. \quad (71)$$

Also, the lower bound of  $\Xi(t_{i+1})$  can be determined from (28) as

$$\|\Xi(t_{i+1})\| \geq \varrho. \quad (72)$$

Therefore, substituting (72) into (71) will results in

$$T_i \geq \frac{1}{k \|\mathcal{J}_0^{-1}\|} \ln \left\{ 1 + \frac{k\varrho}{\Gamma\Omega + k \|\sigma(t_{i+1})\|} \right\} > 0. \quad (73)$$

It has been already established from theorem 1 that  $\omega$  is ultimately bounded within a small region around the origin, and hence the term  $\Gamma\Omega > 0$ . Moreover, the parameters like  $k$ ,  $\varrho$ , and  $\|\mathcal{J}_0^{-1}\|$  are all positive constants. This indicates that all the terms within the natural log in (73) is always greater than 1. Therefore, one can conclude from (73) that  $T_i$  will always be lower bounded by a positive value away from the origin. This completes the proof of theorem 2.  $\square$

## V. SIMULATION AND RESULTS

In this section, the effectiveness of the proposed robust event-triggered attitude control (26) has been demonstrated by numerical simulations for the flexible spacecraft dynamics (5), (22). Furthermore, the performance of the proposed controller has been compared with the existing periodically sampled data technique and the event-trigger based SMC scheme [25] to illustrate the better performance of the proposed scheme. The nominal inertia matrix of the flexible spacecraft is given as:

$$J_0 = \begin{bmatrix} 350 & 3 & 4 \\ 3 & 270 & 10 \\ 4 & 10 & 190 \end{bmatrix} \text{ kg.m}^2, \quad (74)$$

and the parametric uncertainty matrix  $\Delta J$  is considered as [5]

$$\Delta J = \begin{bmatrix} 4.20 & 0.900 & 0.600 \\ 0.900 & -7.00 & 2.50 \\ 0.600 & 2.50 & 5.89 \end{bmatrix} \text{ kg.m}^2. \quad (75)$$

The external disturbances experienced by the spacecraft are taken as [21]

$$d_0(t) = \begin{bmatrix} 1 + 2 \sin(0.005t) \\ -1 - 5 \cos(0.005t) \\ 2 - 4 \sin(0.005t) \end{bmatrix} \times 10^{-4} \text{ N.m.} \quad (76)$$

The coupling matrix of the spacecraft is given as [5]

$$\delta = \begin{bmatrix} 6.45637 & 1.27814 & 2.15629 \\ -1.25619 & 0.91756 & -1.67264 \\ 1.11678 & 2.48901 & -0.83674 \\ 1.23637 & -2.6581 & -1.12503 \end{bmatrix} \text{ kg}^{\frac{1}{2}}.\text{m/s}^2. \quad (77)$$

Table 1 presents the damping ratios and the natural frequencies of the individual elastic mode.

The parameters of the proposed schemes are designed according to [21], [41] which are given as

$$k = \frac{16\bar{\zeta}}{t_s} \|J_0\|_2, \quad k\alpha = \frac{320}{t_s^2} \|J_0\|_2, \quad (78)$$

TABLE 1. Parameters of flexible dynamics [5].

| Mode   | Damping Ratio, $\zeta_i$ | Natural Frequency, $\omega_i$ (rad/s) |
|--------|--------------------------|---------------------------------------|
| Mode 1 | 0.0056                   | 0.7681                                |
| Mode 2 | 0.0086                   | 1.1038                                |
| Mode 3 | 0.013                    | 1.8733                                |
| Mode 4 | 0.025                    | 2.5496                                |

TABLE 2. Controller and system parameters.

| Parameter | $\alpha$ | $\beta$ | $k$ | $\varrho$          |
|-----------|----------|---------|-----|--------------------|
| Value     | 0.2      | 0.5     | 56  | $1 \times 10^{-6}$ |

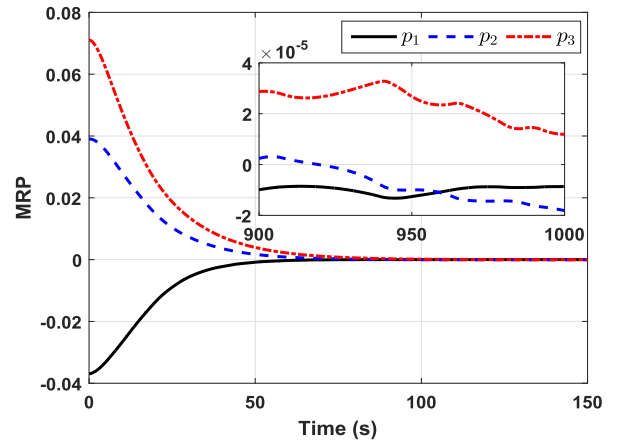


FIGURE 4. Modified Rodrigues parameter response under proposed control (26).

where  $\bar{\zeta} = 1$  is the damping ratio and  $t_s = 100$  s is the settling time. The closed loop parameters are shown in table 2.

The initial conditions of the system states are:

$$p(0) = [-0.037 \ 0.039 \ 0.071]^T \text{ and} \\ \omega(0) = 10^{-3} \times [0.965 \ 0.283 \ 0.151]^T \text{ rad/s.}$$

## A. RESULTS OF THE PROPOSED CONTROLLER

The simulation results under the action of the proposed control scheme are presented in Figs. 4–12. The MRP response is shown in Fig. 4. The trajectories of  $p$  are smoothly converging to the small neighborhood of origin within 100 s of the order  $|p(t)| \leq 2.5 \times 10^{-4}$  under the presence of multiple uncertainties and vibrations. Moreover, the attitude response in Euler angles ( $\phi, \theta, \psi$ ) under the proposed scheme is also presented in Fig. 5. The Euler angles  $\phi, \theta, \psi$  represents the roll, pitch, and yaw angles, respectively. It is evident from Fig. 5 that the Euler angles are also effectively and smoothly converging into the neighborhood of origin within 100 s.

The angular velocity response of the flexible spacecraft is given in Fig. 6. The transient response of  $\omega$  is smooth with the settling time of around 100 s within a bound of  $|\omega(t)| \leq 2.0 \times 10^{-4}$  rad/s. As seen in the enlarged plots of Figs. 4–6, the system states are converging to a very small bound in the neighborhood of origin.

Fig. 7 represents the proposed event-triggered control response (26). It can be observed from Fig. 7 that between the two adjacent triggering instances, the value of  $u(t)$  is kept

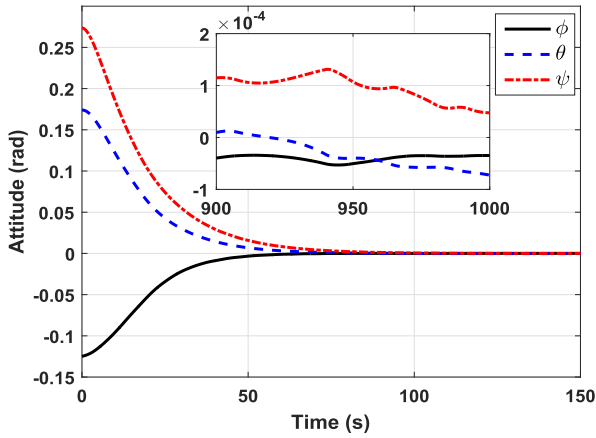


FIGURE 5. Attitude of spacecraft in Euler angle under proposed control (26).

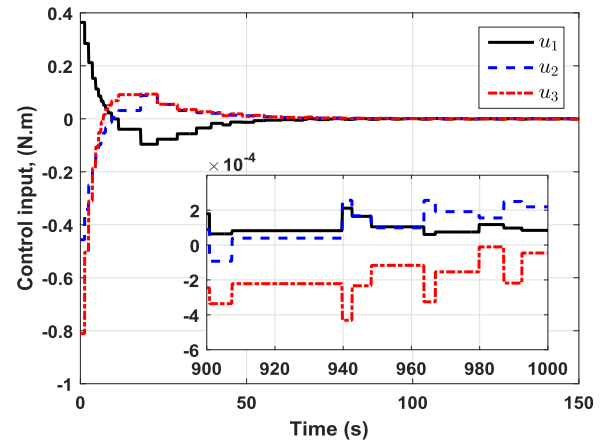


FIGURE 7. The response of the proposed control input torques (26).

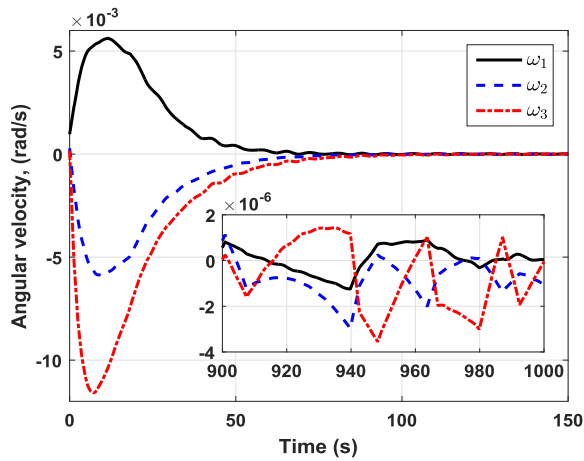


FIGURE 6. Angular velocity response under proposed control (26).

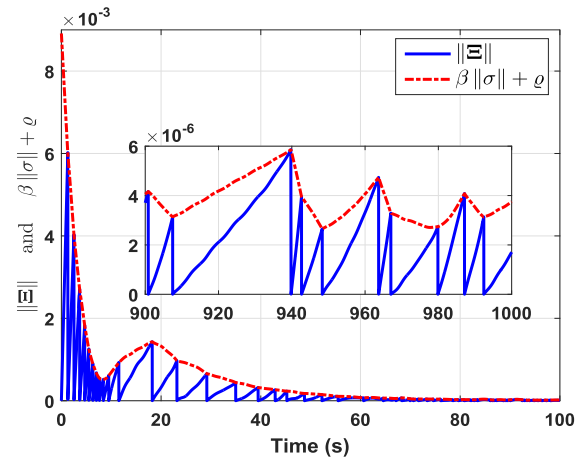


FIGURE 8. The evolution of norm of error  $\|\Xi\|$  and the state dependent parameter  $\beta\|\sigma\| + \varrho$  under the proposed control (26).

the same. The change in the value of  $u(t)$  are occurring when the triggering condition is violated (see Fig. 8). Furthermore, the plot of control input also illustrates the smooth transient response even in the presence of various uncertainties. The control input value converges to a small bound  $|u(t)| \leq 2 \times 10^{-3}$  N.m in 100 s. The number of triggering instants of control input during the whole simulation run of 1000 s is 270. That means the information of  $\sigma$  is updated 270 times through the communication channel.

The time response of  $\|\Xi\|$  and the triggering condition  $\beta\|\sigma\| + \varrho$  are shown in Fig. 8. As seen in Fig. 8, whenever  $\|\Xi\| = \beta\|\sigma\| + \varrho$ , then in the next iteration the value of  $\|\Xi\|$  becomes 0. This is due to the update in the value of  $\sigma(t_i)$  to the current value of  $\sigma(t)$  as described in (27). The settling time of state dependent parameter  $\beta\|\sigma\| + \varrho$  to the neighborhood of zero is around 80 s. The steady state response of both the parameters are shown in the magnified plot in Fig. 8 which shows  $\varrho < \|\Xi\| \leq 1 \times 10^{-5}$  and agreeing with (72).

The time history of feedback vector  $\sigma(t)$  is presented in Fig. 9. As seen from Fig. 9, the trajectories of  $\sigma(t)$  converges to a small neighborhood of zero within 100 s.

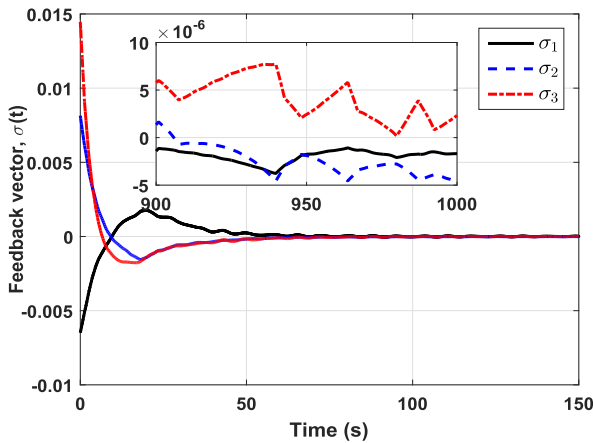
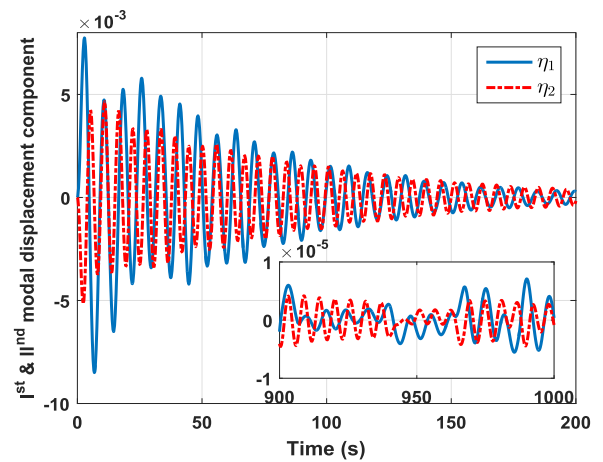
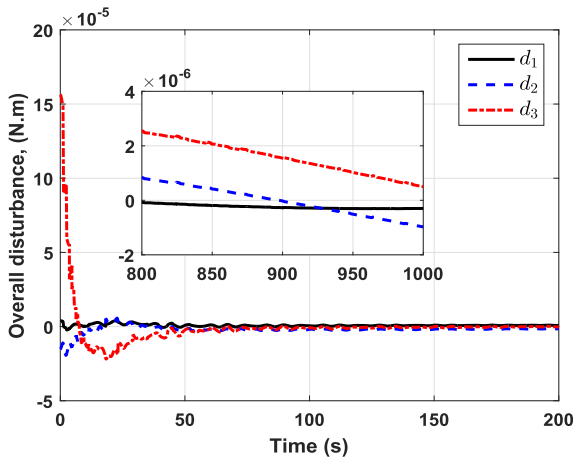
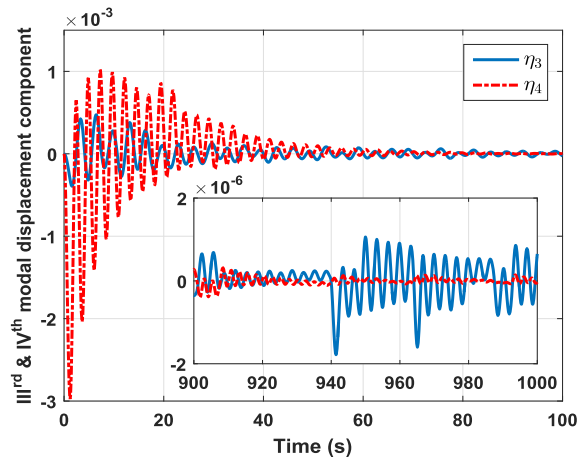
The bound of  $\sigma(t)$  during the steady state is  $2 \times 10^{-5}$ . The plot of overall disturbance experienced by the flexible spacecraft is depicted in Fig. 10. It is evident from Fig. 10 that under the action of the proposed controller, the overall disturbance is effectively reduces to a very small bound in the range of  $2 \times 10^{-5}$  N.m within 50 s. The steady state response of disturbance is also shown in the enclosed plot in Fig. 10 which is within the range of  $5 \times 10^{-6}$  N.m.

Furthermore, the displacement of the flexible modes are displayed in Fig. 11 and 12. The proposed controller converges the vibrations of flexible modal  $\eta$  to a small magnitude of less than  $4 \times 10^{-3}$  in 50 s. The time of convergence of  $\eta$  can further be reduced by using sufficiently large controller gain. The Euclidean norm of vector  $\eta$  during the steady state is  $2.6 \times 10^{-4}$ . Moreover, the energy utilized to regulate the spacecraft is measured using the energy index function defined as  $E = \sum_{i=1}^3 \int_0^t |u_i(\tau)|^2 d\tau$ . The proposed controller achieves the desired attitude by using the energy of  $2.56 \text{ N}^2\text{m}^2$ .

The steady state performance of the spacecraft under the proposed controller (26) is summarized in Table 3. In addition, Table 3 shows the system performance under different

**TABLE 3.** System performance under the proposed control (26) at different values of parameter  $\varrho$  during the steady state.

| Parameter $\varrho$ | Avg $T_i$ (s) | No. of trans. | $\ \omega\ _2$       | $\ p\ _2$            | $\ \eta\ _2$         | Energy ( $N^2m^2$ ) |
|---------------------|---------------|---------------|----------------------|----------------------|----------------------|---------------------|
| $1 \times 10^{-6}$  | 3.68          | 270           | $1.6 \times 10^{-4}$ | $2.8 \times 10^{-3}$ | $2.6 \times 10^{-4}$ | 2.56                |
| $1 \times 10^{-5}$  | 5.58          | 178           | $4.9 \times 10^{-4}$ | $3.2 \times 10^{-3}$ | $4.0 \times 10^{-3}$ | 2.56                |
| $1 \times 10^{-4}$  | 10.08         | 97            | $5.4 \times 10^{-3}$ | $1.3 \times 10^{-2}$ | $1.5 \times 10^{-2}$ | 2.59                |

**FIGURE 9.** The response of the feedback vector trajectory (25).**FIGURE 11.** Modal displacement of  $\eta_1$  and  $\eta_2$ .**FIGURE 10.** Overall disturbances subjected to the flexible spacecraft (23).**FIGURE 12.** Modal displacement of  $\eta_3$  and  $\eta_4$ .

values of the parameter  $\varrho$ . It can be observed from the Table 3 that with the smaller value of  $\varrho$ , the system performance is better at the cost of higher number of triggering instants and vice versa. Therefore, one has to identify the controller constraints and specifications while selecting the appropriate value of  $\varrho$  to achieve the desired performance objective.

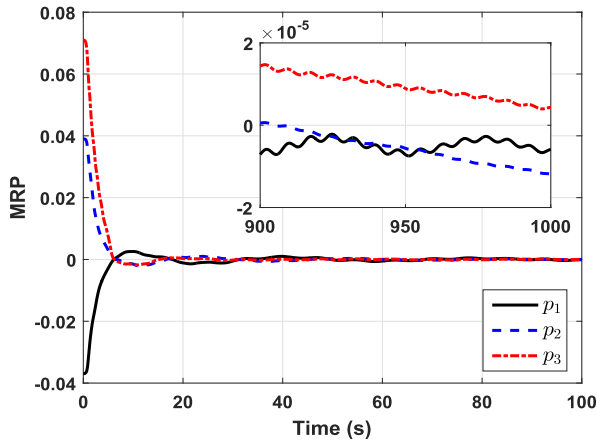
## B. RESULTS OF THE PERIODICALLY SAMPLED DATA TECHNIQUE

For comparison, the traditional periodically sampled data technique is also simulated for the same initial conditions and the controller gain  $k$ . The corresponding control structure is similar to (26) and the only difference is that the control is updated at a fixed sample time  $T$  and not according to the

event triggering condition (28). The performance of periodically sampled data technique for the attitude regulation at different sampling time is presented in Table 4. It can be seen from the first row of measurements in both the Table 3 and 4, the performance of the periodically sampled data technique is slightly better than the proposed controller but at the cost of higher number of transmissions (i.e., the control is updated 230 times more through wireless network) and  $0.36 N^2m^2$  of more energy than the proposed scheme (26). Furthermore, as the sampling time increases in Table 4, the performance of the periodically sampled data technique degrades and also it consumes more energy. In contrast, the proposed methodology (26) achieves the satisfactory results even with only

**TABLE 4.** System performance using periodically sampled data technique at different sampling time  $T$  during the steady state.

| Periodic time (s) | No. of trans. | $\ \omega\ _2$       | $\ p\ _2$            | $\ \eta\ _2$         | Energy ( $\text{N}^2\text{m}^2$ ) |
|-------------------|---------------|----------------------|----------------------|----------------------|-----------------------------------|
| 2                 | 500           | $1.1 \times 10^{-4}$ | $2.3 \times 10^{-3}$ | $4.2 \times 10^{-6}$ | 2.92                              |
| 3                 | 333           | $1.1 \times 10^{-4}$ | $2.3 \times 10^{-3}$ | $1.4 \times 10^{-4}$ | 3.58                              |
| 4                 | 250           | $3.0 \times 10^{-3}$ | $2.3 \times 10^{-2}$ | 0.14                 | 4.67                              |
| 4.5               | 222           | $1.5 \times 10^{-1}$ | $4.9 \times 10^{-2}$ | 7.57                 | 10.55                             |

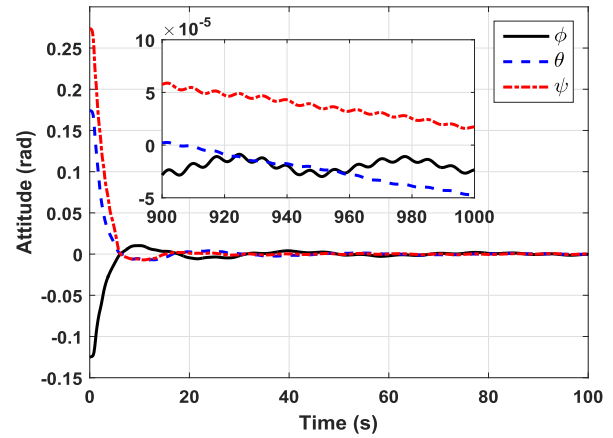
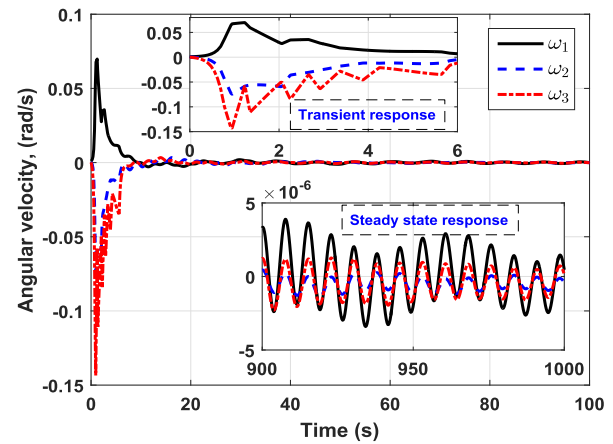
**FIGURE 13.** Modified Rodrigues parameter response under the control algorithm of [25].

97 updates of the control input. Moreover, there is no significant change in the energy consumption for all the simulation results under the proposed scheme as shown in Table 3. Therefore, it is evident that under the constraint of limited transmission, the proposed control (26) is performing better than the periodically sampled data technique.

### C. RESULTS OF THE EVENT-TRIGGERED SMC

Another comparative simulation analysis is performed with a recently proposed controller on the event-triggered SMC [25]. The event-triggered control law is designed using a linear sliding surface structure  $s = \omega + Kp$  where  $K = \text{diag}[2 \ 2 \ 2]$ . The triggering condition is expressed as:  $t_{i+1} = \inf\{t : t > t_i, \|e(t)\|_1 \geq \epsilon \|\omega(t_i)\|_1 + r\}$  where  $e(t) = \omega(t_i) - \omega(t)$ ,  $\epsilon = 0.5$ , and  $r = 1 \times 10^{-6}$ . The control law is given as  $u = -\{J^* \mu \|\omega(t_i)\|_1 + C(\omega(t_i))\} \text{sign}(s(t_i))$  for all  $t \in [t_i, t_{i+1})$ . The parameter  $C(\omega(t_i))$  and the signum function  $\text{sign}(s(t_i))$  are sampled at every triggering instant  $t_i$ . The parameter  $C(\omega(t_i))$  is defined as  $C(\omega(t_i)) \geq d_{\max} + \alpha_1 + \beta_1 \|\omega(t_i)\|_1$  where  $J^* = 360$ ,  $\mu = 3$ ,  $d_{\max} = 1$ ,  $\alpha_1 = 0.001$ ,  $\beta_1 = 530$ .

The simulation results under the control algorithm of [25] are presented in Figs. 13–20. The attitude states in terms of MRP and Euler angles are illustrated in Fig. 13 and 14, respectively whereas the angular velocity is presented in Fig. 15. Although the transient response of the system trajectories is fast due to the high magnitude of control input (see Fig. 16), the behavior of the transient response is not smooth and even in 100 s, the system states are only able to converge within a bound of  $\|p(t)\| \leq 7.4 \times 10^{-3}$  and  $\|\omega(t)\| \leq 1.2 \times 10^{-2}$  rad/s.

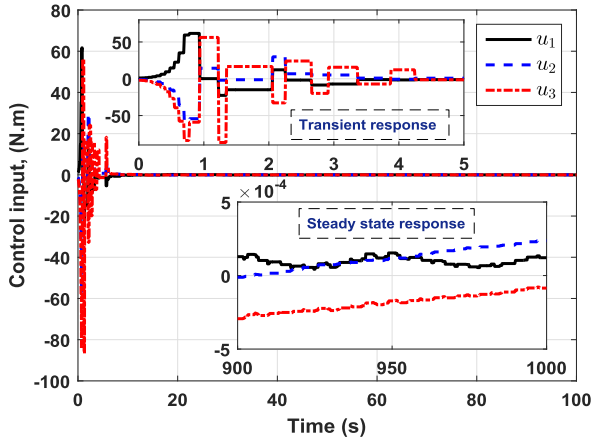
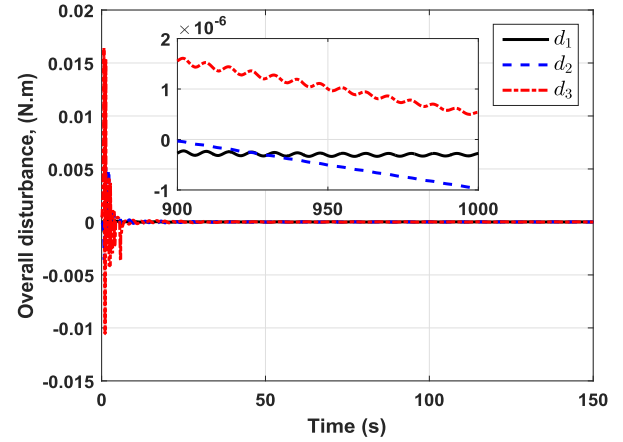
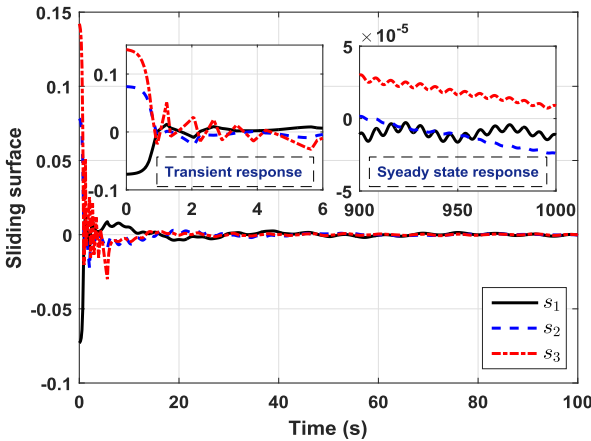
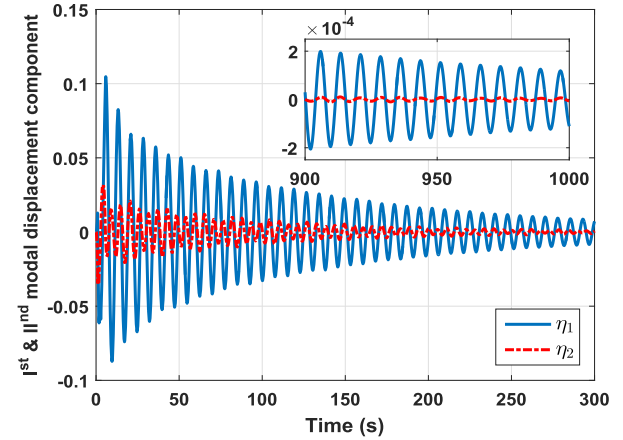
**FIGURE 14.** Attitude of spacecraft in Euler angle under the control algorithm of [25].**FIGURE 15.** Angular velocity response under the control algorithm of [25].

The magnitudes of the control input during the transient response in Fig. 16 are too high compared to the proposed controller (Fig. 7). The value of the control input converges to a bound  $|u(t)| \leq 6 \times 10^{-3}$  N.m in 100 s. The energy utilized under this scheme is  $6.96 \times 10^3$   $\text{N}^2\text{m}^2$  which is too excessive compared to the proposed technique. Furthermore, the control law is updated 2118 times through communication channel in 1000 s, which is too high as compared to the proposed technique. The control algorithm of [25] ultimately loses the objective of minimal utilization of energy and communication resources with this high magnitude and high rate of data transmission.

The sliding surface response is presented in Fig. 17. The transient response of the sliding surface is non-smooth, and it takes approximately 60 s for  $s$  to converge in the vicinity of origin with a bound  $1 \times 10^{-3}$ . The steady-state convergence accuracy of  $s$  is  $\leq 8 \times 10^{-5}$ . The initial magnitude of the overall disturbance, as shown in Fig. 18, is also high due to the high magnitude of control input. In the proposed technique (26), the maximum value of  $d$  is less than  $2 \times 10^{-4}$  N.m, whereas in case of [25], it reaches to  $1.7 \times 10^{-2}$  N.m. During the steady state,  $d$  is limited within the bound of  $3 \times 10^{-6}$  N.m as seen from the steady-state response given within Fig. 18.

**TABLE 5.** System performance under the control algorithm of [25] at different values of parameter  $r$  during the steady state.

| Parameter $r$      | Avg $T_i$ (s) | No. of trans. | $\ \omega\ _2$       | $\ p\ _2$            | $\ \eta\ _2$         | Energy ( $\text{N}^2\text{m}^2$ ) |
|--------------------|---------------|---------------|----------------------|----------------------|----------------------|-----------------------------------|
| $1 \times 10^{-6}$ | 0.47          | 2118          | $2.0 \times 10^{-4}$ | $1.2 \times 10^{-3}$ | $1.1 \times 10^{-2}$ | $6.96 \times 10^3$                |
| $1 \times 10^{-5}$ | 0.68          | 1168          | $2.1 \times 10^{-3}$ | $4.7 \times 10^{-3}$ | $5.7 \times 10^{-2}$ | $7.84 \times 10^3$                |

**FIGURE 16.** The response of the control input torque under the control algorithm of [25].**FIGURE 18.** Overall disturbances subjected to the flexible spacecraft (23) under the control algorithm of [25].**FIGURE 17.** The response of the sliding surface under the control algorithm of [25].**FIGURE 19.** Modal displacement of  $\eta_1$  and  $\eta_2$  under the control algorithm of [25].

The modal displacement responses of the first two and the last two components are shown in Fig. 19 and 20, respectively. It is evident from Fig. 19 that  $\eta_1$  is settling down to a magnitude of  $5 \times 10^{-2}$  in 50 s which is a higher value as compared to the proposed scheme where  $|\eta_1| \leq 5 \times 10^{-3}$  in 50 s (Fig. 11). Moreover, during the steady state, the proposed controller is performing better than the control of [25] in suppressing the vibration of flexible modes to a smaller bound. The Euclidean norm of vector  $\eta$  during the steady state is  $1.1 \times 10^{-2}$ , whereas in case of the proposed technique (26), it is  $2.6 \times 10^{-4}$ .

The performance of the control algorithm of [25] is summarized in Table 5. Similar to the proposed technique, the control of [25] is also tested under different values of

parameter  $r$  and its performance is also tabulated in Table 5. Unlike the proposed scheme where the controller exhibits acceptable performance even with  $\varrho = 1 \times 10^{-4}$ , the control performance of [25] gets deteriorate with  $r > 1 \times 10^{-5}$ . The scheme of [25] consumes more communication resources by utilizing high control updating frequency than the proposed scheme. For instance from Table 5 with  $r = 1 \times 10^{-5}$ , the controller updates the input 1168 times with an average  $T_i = 0.68$  s. On the other hand in Table 3 with  $\varrho = 1 \times 10^{-5}$ , the proposed controller updates the input 178 times with an average  $T_i = 10.08$  s. Even then the performance of the proposed scheme is better than the scheme of [25].

It is observed based upon the above simulation results that although the algorithm of [25] generates a faster transient response by consuming more control input, the proposed

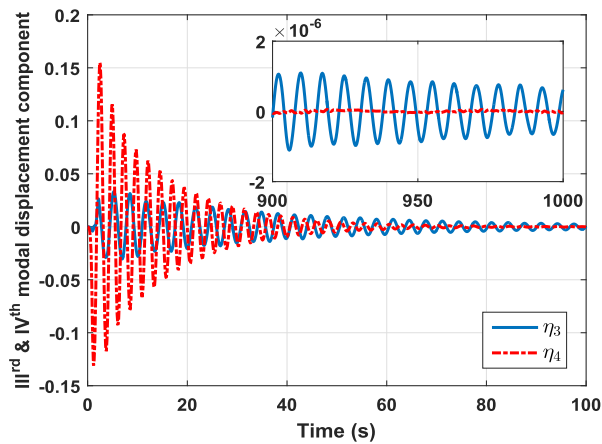


**FIGURE 20.** Modal displacement of  $\eta_3$  and  $\eta_4$  under the control algorithm of [25].

technique (26) exhibits smooth transient response and better steady state performance by utilizing lesser energy and data transmission. Moreover, the proposed controller is effectively suppressing the flexible vibrations to a smaller convergence bound than the control scheme of [25].

## VI. CONCLUSION

This paper designed a robust event-triggered attitude regulation control of the flexible spacecraft where the attitudes are represented by MRP. The spacecraft has the constraint of limited utilization of control updating frequency. Furthermore, the spacecraft is subjected to the parametric uncertainties, external disturbances, and flexible modal vibrations due to solar appendages. The proposed controller is developed by using a novel state dependent feedback vector. The information of the feedback vector gets updated to the on-board attitude controller whenever the predefined triggering condition is satisfied. The stability of the closed-loop system using the Lyapunov theory guarantees the UUB convergence of system states where the system state reside in the small bounds near the neighborhood of origin. Moreover, it is also proved that the inter-update time under the proposed methodology is always lower bounded by a positive value which establishes that the proposed scheme is free from the Zeno behavior. Finally, the numerical simulation results illustrate the effectiveness and validity of the proposed control approach under various uncertainties and disturbances. Few potential future extension of this work could be: incorporating the adaptive based event-trigger control, extending this approach for the attitude tracking problem, etc.

## ACKNOWLEDGMENT

This publication was made possible by Qatar University High Impact grant # [QUHI-CENG-19/20-2] from the Qatar University. The statements made herein are solely the responsibility of the authors. The publication charges are paid by the Qatar National Library, Doha, Qatar.

## REFERENCES

- [1] K. Lu and Y. Xia, "Finite-time attitude stabilization for rigid spacecraft," *Int. J. Robust Nonlinear Control*, vol. 25, no. 1, pp. 32–51, Jan. 2015.
- [2] D. Lee, "Nonlinear disturbance observer-based robust control of attitude tracking of rigid spacecraft," *Nonlinear Dyn.*, vol. 88, no. 2, pp. 1317–1328, Apr. 2017.
- [3] P. M. Tiwari, S. Janardhanan, and M. Un-Nabi, "Spacecraft anti-unwinding attitude control using second-order sliding mode," *Asian J. Control*, vol. 20, no. 1, pp. 455–468, 2018.
- [4] C. Liu, Z. Sun, D. Ye, and K. Shi, "Robust adaptive variable structure tracking control for spacecraft chaotic attitude motion," *IEEE Access*, vol. 6, pp. 3851–3857, 2018.
- [5] S. D. Gennaro, "Output stabilization of flexible spacecraft with active vibration suppression," *IEEE Trans. Aerosp. Electron. Syst.*, vol. 39, no. 3, pp. 747–759, Jul. 2003.
- [6] S. Xu, N. Cui, Y. Fan, and Y. Guan, "Active vibration suppression of flexible spacecraft during attitude maneuver with actuator dynamics," *IEEE Access*, vol. 6, pp. 35327–35337, 2018.
- [7] H. Liu, L. Guo, and Y. Zhang, "An anti-disturbance PD control scheme for attitude control and stabilization of flexible spacecrafts," *Nonlinear Dyn.*, vol. 67, no. 3, pp. 2081–2088, 2012.
- [8] H. Bang, C.-K. Ha, and J. H. Kim, "Flexible spacecraft attitude maneuver by application of sliding mode control," *Acta Astronautica*, vol. 57, no. 11, pp. 841–850, Dec. 2005.
- [9] Q.-L. Hu, Z. Wang, and H. Gao, "Sliding mode and shaped input vibration control of flexible systems," *IEEE Trans. Aerosp. Electron. Syst.*, vol. 44, no. 2, pp. 503–519, Apr. 2008.
- [10] Q. Hu, "Robust adaptive sliding mode attitude control and vibration damping of flexible spacecraft subject to unknown disturbance and uncertainty," *Trans. Inst. Meas. Control*, vol. 34, no. 4, pp. 436–447, 2012.
- [11] Y. Jiang, Q. Hu, and G. Ma, "Adaptive backstepping fault-tolerant control for flexible spacecraft with unknown bounded disturbances and actuator failures," *ISA Trans.*, vol. 49, no. 1, pp. 57–69, 2010.
- [12] B. Xiao, Q. Hu, and Y. Zhang, "Adaptive sliding mode fault tolerant attitude tracking control for flexible spacecraft under actuator saturation," *IEEE Trans. Control Syst. Technol.*, vol. 20, no. 6, pp. 1605–1612, Nov. 2012.
- [13] Y. Ma, B. Jiang, G. Tao, and Y. Cheng, "Uncertainty decomposition-based fault-tolerant adaptive control of flexible spacecraft," *IEEE Trans. Aerosp. Electron. Syst.*, vol. 51, no. 2, pp. 1053–1068, Apr. 2015.
- [14] S. Wu, W. Chu, X. Ma, G. Radice, and Z. Wu, "Multi-objective integrated robust H $\infty$  control for attitude tracking of a flexible spacecraft," *Acta Astronautica*, vol. 151, pp. 80–87, Oct. 2018.
- [15] R. Yan and Z. Wu, "Attitude stabilization of flexible spacecrafts via extended disturbance observer based controller," *Acta Astronautica*, vol. 133, pp. 73–80, Apr. 2017.
- [16] Y. Miao, F. Wang, and M. Liu, "Anti-disturbance backstepping attitude control for rigid-flexible coupling spacecraft," *IEEE Access*, vol. 6, pp. 50729–50736, 2018.
- [17] B. Wu, "Spacecraft attitude control with input quantization," *J. Guid., Control, Dyn.*, vol. 39, no. 1, pp. 176–181, Aug. 2015.
- [18] P. Tabuada, "Event-triggered real-time scheduling of stabilizing control tasks," *IEEE Trans. Autom. Control*, vol. 52, no. 9, pp. 1680–1685, Sep. 2007.
- [19] A. Sahoo, H. Xu, and S. Jagannathan, "Adaptive neural network-based event-triggered control of single-input single-output nonlinear discrete-time systems," *IEEE Trans. Neural Netw. Learn. Syst.*, vol. 27, no. 1, pp. 151–164, Jan. 2016.
- [20] J. F. Guerrero-Castellanos, J. J. Téllez-Guzmán, S. Durand, N. Marchand, J. U. Alvarez-Muñoz, and V. R. González-Díaz, "Attitude stabilization of a quadrotor by means of event-triggered nonlinear control," *J. Intell. Robot. Syst.*, vol. 73, nos. 1–4, pp. 123–135, 2014.
- [21] B. Wu, Q. Shen, and X. Cao, "Event-triggered attitude control of spacecraft," *Adv. Space Res.*, vol. 61, no. 3, pp. 927–934, 2018.
- [22] C. Zhang, J. Wang, D. Zhang, and X. Shao, "Learning observer based and event-triggered control to spacecraft against actuator faults," *Aerosp. Sci. Technol.*, vol. 78, pp. 522–530, Jul. 2018.
- [23] C. Zhang, J. Wang, R. Sun, D. Zhang, and X. Shao, "Multi-spacecraft attitude cooperative control using model-based event-triggered methodology," *Adv. Space Res.*, vol. 62, no. 9, pp. 2620–2630, 2018.
- [24] S. Weng, D. Yue, X. Xie, and Y. Xue, "Distributed event-triggered cooperative attitude control of multiple groups of rigid bodies on manifold SO(3)," *Inf. Sci.*, vols. 370–371, pp. 636–649, Nov. 2016.
- [25] Y. Liu, B. Jiang, J. Lu, J. Cao, and G. Lu, "Event-triggered sliding mode control for attitude stabilization of a rigid spacecraft," *IEEE Trans. Syst., Man, Cybern., Syst.*, to be published.

- [26] B. Huang, A.-J. Li, Y. Guo, and C.-Q. Wang, "Fixed-time attitude tracking control for spacecraft without unwinding," *Acta Astronautica*, vol. 151, pp. 818–827, Oct. 2018.
- [27] H. Schaub and J. L. Junkins, "Stereographic orientation parameters for attitude dynamics: A generalization of the Rodrigues parameters," *J. Astron. Sci.*, vol. 44, no. 1, pp. 1–19, 1996.
- [28] M. R. Binette, C. J. Damaren, and L. Pavel, "Nonlinear  $H_\infty$  attitude control using modified Rodrigues parameters," *J. Guid., Control, Dyn.*, vol. 37, no. 6, pp. 2017–2021, 2014.
- [29] C. D. Karlgaard and H. Schaub, "Nonsingular attitude filtering using modified Rodrigues parameters," *J. Astron. Sci.*, vol. 57, no. 4, pp. 777–791, Oct. 2009.
- [30] H. Schaub, J. L. Junkins, and R. D. Robinett, "New penalty functions and optimal control formulation for spacecraft attitude control problems," *J. Guid., Control, Dyn.*, vol. 20, no. 3, pp. 428–434, 1997.
- [31] H. Schaub, M. R. Akella, and J. L. Junkins, "Adaptive control of nonlinear attitude motions realizing linear closed loop dynamics," *J. Guid. Control Dyn.*, vol. 24, no. 1, pp. 95–100, Jan. 2001.
- [32] Z. Wang and Z. Wu, "Nonlinear attitude control scheme with disturbance observer for flexible spacecrafts," *Nonlinear Dyn.*, vol. 81, nos. 1–2, pp. 257–264, 2015.
- [33] C. Pukdeboon and A. Jitpattanakul, "Anti-unwinding attitude control with fixed-time convergence for a flexible spacecraft," *Int. J. Aerosp. Eng.*, vol. 2017, Aug. 2017, Art. no. 5018323.
- [34] Z. Zhu, Y. Xia, and M. Fu, "Adaptive sliding mode control for attitude stabilization with actuator saturation," *IEEE Trans. Ind. Electron.*, vol. 58, no. 10, pp. 4898–4907, Oct. 2011.
- [35] K. Ma, "Comments on 'Quasi-continuous higher order sliding-mode controllers for spacecraft-attitude-tracking maneuvers,'" *IEEE Trans. Ind. Electron.*, vol. 60, no. 7, pp. 2771–2773, Jul. 2013.
- [36] C. Pukdeboon, "Adaptive-gain second-order sliding mode control of attitude tracking of flexible spacecraft," *Math. Problems Eng.*, vol. 2014, May 2014, Art. no. 312494.
- [37] R. Yan and Z. Wu, "Finite-time attitude stabilization of flexible spacecrafts via reduced-order SMDO and NTSMC," *J. Aerosp. Eng.*, vol. 31, no. 4, 2018, Art. no. 04018023.
- [38] S. Ding and W. X. Zheng, "Nonsmooth attitude stabilization of a flexible spacecraft," *IEEE Trans. Aerosp. Electron. Syst.*, vol. 50, no. 2, pp. 1163–1181, Apr. 2014.
- [39] R. Postoyan, P. Tabuada, D. Nešić, and A. Anta, "A framework for the event-triggered stabilization of nonlinear systems," *IEEE Trans. Autom. Control*, vol. 60, no. 4, pp. 982–996, Apr. 2015.
- [40] H. K. Khalil, *Nonlinear Systems*, vol. 3. Noida, India: Pearson, 2014.
- [41] B. Wie, H. Weiss, and A. Arapostathis, "Quaternion feedback regulator for spacecraft eigenaxis rotations," *J. Guid., Control, Dyn.*, vol. 12, no. 3, pp. 375–380, May 1989.



include nonlinear control, sliding mode control, robust control, spacecraft attitude control, renewable energy, and power electronics.

**SYED MUHAMMAD AMRR** (S'18) received the bachelor's degree in electrical engineering and the master's degree in instrumentation and control from the Department of Electrical Engineering, Aligarh Muslim University (AMU), Aligarh, India, in 2014 and 2016, respectively. He is currently pursuing the Ph.D. degree with the Control and Automation Group, Department of Electrical Engineering, Indian Institute of Technology Delhi (IITD), New Delhi, India. His research interests



Associate Professor. His research interests mainly include reduced order modeling (model order reduction), optimal control, sliding mode control, neuro-fuzzy control, and computational electromagnetics.

**MASHUQ UN NABI** (M'10) received the B.E. degree in electrical engineering from Jadavpur University, Kolkata, India, in 1997, the M.Tech. degree in electrical engineering from the Indian Institute of Technology Kanpur (IITK), India, in 1999, and the Ph.D. degree from the Indian Institute of Technology Bombay (IITB), India, in 2004. He joined the Department of Electrical Engineering, Indian Institute of Technology Delhi (IITD), in 2005, where he is currently an



**ATIF IQBAL** (M'08–SM'11) received the B.Sc. degree (Hons.) and the M.Sc. engineering degree in power system and drives from Aligarh Muslim University (AMU), Aligarh, India, in 1991 and 1996, respectively, and the Ph.D. degree from Liverpool John Moores University, Liverpool, U.K., in 2006. He has been a Lecturer with the Department of Electrical Engineering, AMU, since 1991, where he was a Full Professor, until 2016. He is currently an Associate Professor with the Electrical Engineering Department, Qatar University. He has published widely in international journals and conferences his research findings related to power electronics and renewable energy sources. He has authored/coauthored more than 350 research papers, one book, and three chapters in two other books. He has supervised several large Research and Development projects. His research interests include modeling and simulation of power electronic converters, control of multi-phase motor drives, and renewable energy sources. He is a Fellow of IET (U.K.), and Fellow of IE (India). He was a recipient of Outstanding Faculty Merit Award AY 2014–2015, Research Excellence Award at Qatar University, Doha, Qatar, and Maulana Tufail Ahmad Gold Medal for standing first at B.Sc. Engg. Exams from AMU, in 1991. He has received best research papers awards at the IEEE ICIT-2013, IET SEISCON-2013, and SIGMA 2018. He is an Associate Editor of the IEEE TRANSACTIONS ON INDUSTRY APPLICATION and IEEE ACCESS, and the Editor-in-Chief of I'manager's *Journal of Electrical Engineering*.

...